magnetochemistry

MDPI

Article

Supplementary Information on: Diamagnetism of Bulk Graphite Revised

Bogdan Semenenko and Pablo D. Esquinazi *

Division of Superconductivity and Magnetism, Felix-Bloch-Institute for Solid State Physics, Faculty of Physics and Earth Sciences, University of Leipzig, Linnéstraße 5, 04103 Leipzig, Germany; semenenko@studserv.uni-leipzig.de (B.S.)

* Correspondence: esquin@physik.uni-leipzig.de; Tel.: +49-341-97-32-751

Received: 15 October 2018; Accepted: 16 November 2018; Published: date

1. Comparison between the Thickness Dependence of the Susceptibility and of the Electrical Conductivity at 4 K and 300 K

Figure S1 shows similar data as Figure 4 of the main text, but including the conductivity data at 4 K of the selected graphite samples. Note that the smaller the sample thickness, the temperature dependence of the conductivity changes from metallic-like (at large enough thickness) to semiconducting-like at thicknesses less than $\sim$ 50 nm [1]. This means that we expect a crossover at a small enough thickness between the two series of data (4 K and 300 K), as seen in the figure.

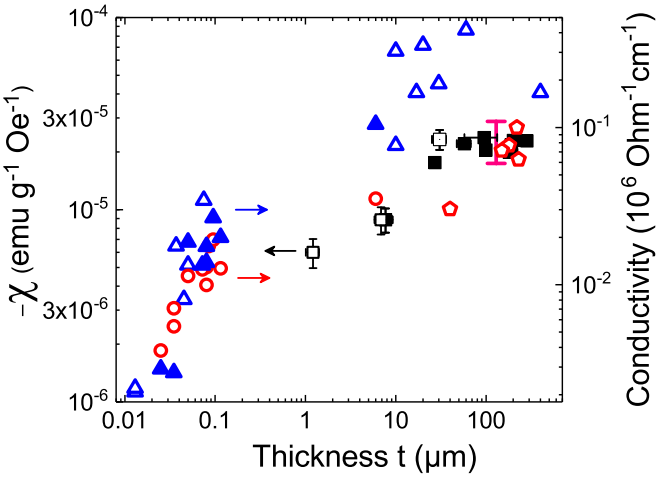

Figure S1. c-axis susceptibility of different graphite samples vs. their thickness at 300 K measured by a torquemeter (□) and a SQUID magnetometer (■). The samples were obtained from precharacterized bulk natural graphite, as well as HOPG of Grade ZYA samples. The HOPG sample with a thickness 30.6 μm was measured with SQUID and torque magnetometers (⊡). The vertical error bar at the top right indicates the values reported for differently oriented samples in the literature [2–8] at 300 K. Right y-axis: thickness dependence of the conductivity of several bulk and thin graphite samples taken at 300 K (○) and 4 K (▲) from [1], at 300 K (⬠) from [9], at 4 K (△) from [1,10–14], and calculated taking the measured geometry in those publications.

2. Surface to Volume Ratio

The results shown in Figure S2 indicate that the decrease in the susceptibility is not related to a decrease of the total S_{total} or the lateral $S_{lateral}$ sample area. The observed behavior is related solely to a decrease in the thickness, as expected from the microstructure of the graphite samples [15].

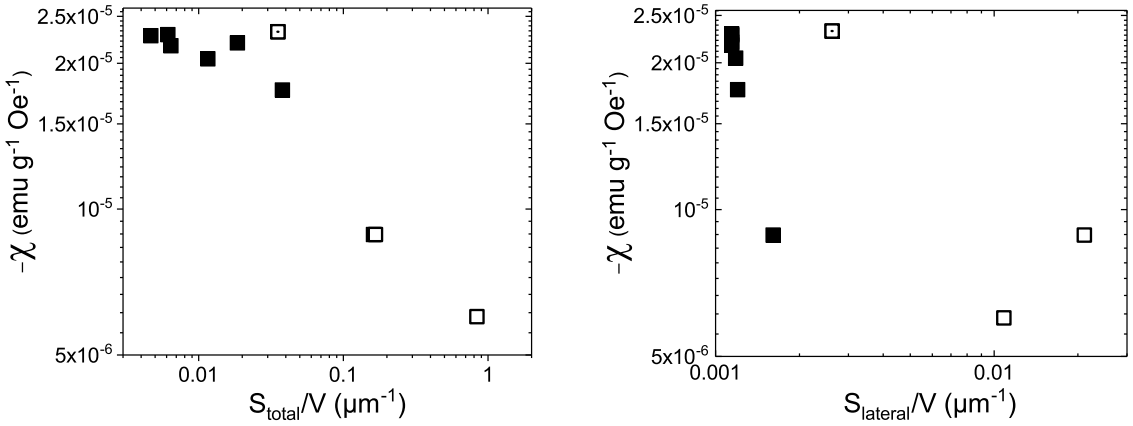

Figure S2. Susceptibility vs. (**a**) the ratio between the total surface and volume and (**b**) the ratio between the lateral surface and volume of the graphite samples, measured with a SQUID magnetometer (■, ⊡) and torque magnetometers (⊡, □).

3. Particle-Induced X-Ray Emission Characterization of the Samples' Impurities

For the measurement of the susceptibility, we have selected HOPG ZYA graphite samples, which were previously characterized by PIXE (penetration depth of $\sim$ 35 μm) at the surface and at the sides; see [16]. ZYA samples are the ones with the highest structural quality and have the lowest Fe concentration < 1 μg/g, and the concentration of other magnetic elements is much smaller. One should take care that the side surfaces can show a higher impurity concentration [16] than in bulk. Therefore, one should clean with ultrasound before using them and prepare the flakes. The graphite flakes show an even smaller impurity concentration than the bulk samples, in general. However, the measuring error increases due to the small mass of the flakes.

The impurity content of the natural graphite samples was determined also by PIXE; see [17]. It is important in this case to remove the first hundreds of nanometers from the as-received surface, which usually have some extra contamination. The clean surfaces, as well as in the bulk showed a concentration of ~ 6 μg/g of Fe and of Ti. The other elements' concentrations were below the detection limit. Similar to the HOPG samples, we did not find any increase in the impurity concentration by decreasing the thickness of the samples, i.e., the impurities were in general homogeneously distributed in the samples.

The magneto-transport properties of thin graphite flakes, thoroughly studied in the past [10,18–20], did not show any sign of negative magnetoresistance, a fingerprint of magnetic scattering [21]. Therefore, we can rule out the possibility that due to the decrease of the sample thickness, we have an increase of the paramagnetic or ferromagnetic contribution as the reason for the decrease in the total diamagnetic susceptibility.

4. Original Experimental Data and the Calibration Curve

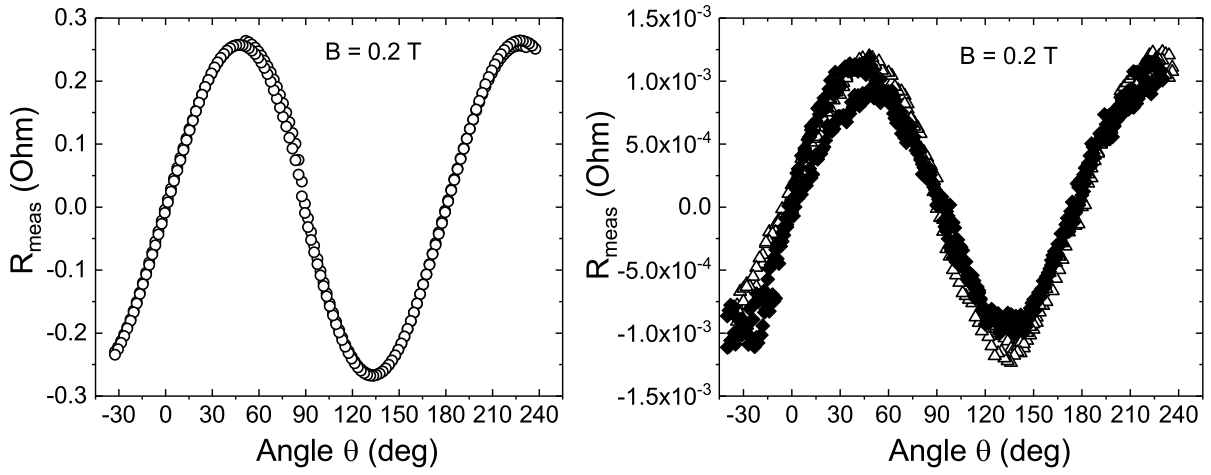

a) b)

Figure S3. Measured resistance signal vs. angle θ between the applied field and the c-axis of the graphite samples with thicknesses: (**a**) 30.6 μm (○), (**b**) 6.9 μm (△), and 1.2 μm (♦).

Figure S3 shows the original experimental data taken from three graphite flakes with different thicknesses. Measurements of the resistance signal were carried out depending on the angle θ between the constant magnetic field B and the c-axis of the graphite samples. The applied magnetic field was 0.2 T (= 2 kOe). Note that each curve was taken with different cantilevers with different spring constants k and gauge factors GF (see Table 1).

Table 1. Table with the parameters of the cantilevers used for the magnetometry.

Cantilever No.	l (μm)	w (μm)	t_c (μm)	k (N/m)	R_0 (kOhm)	GF	measured sample and sample thickness
153 (4)	305	110	5.1	22.6	1.206	1.57	NG No.13, t = 6.9 μm
189 (2)	305	110	3.8	8.7	1.212	1.75	NG No.16, t = 1.2 μm
101 (5b)	305	110	4.3	12.7	1.169	0.84	HOPG, t = 30.6 μm

To estimate the susceptibility of the graphite samples, we did the following calculations. The accuracy of these estimates was checked by comparing the measured susceptibility of the same sample with the SQUID and a torque magnetometer. The torque that arises from a sample with a magnetic moment m in an applied magnetic field B is equal to:

$$\vec{\tau} = \vec{m} \times \vec{B}, \tag{1}$$

or:

$$\tau = mB\sin(\theta), \tag{2}$$

where θ is the angle between the magnetic moment m and the applied magnetic field B. Because graphite is a strong anisotropic material ($\chi_{\parallel} >> \chi_{\perp}$), its magnetic moment can be written as:

$$m = \chi_{\parallel} m_m B\cos(\theta), \tag{3}$$

where $\chi_{\parallel}$ is the mass magnetic susceptibility for a field applied parallel to the c-axis of graphite and m_m is the mass of the sample.

Thus, taking into account Equations 2 and 3, the final formula of the torque will be as follows (identical to that obtained in [22]):

$$\tau = \chi_{\parallel} m_m B^2 \cos(\theta) \sin(\theta) = \frac{1}{2} \chi_{\parallel} m_m B^2 \sin(2\theta) \tag{4}$$

The torque of the anisotropic sample will create a force $\vec{F}$ acting on the tip of the cantilever of length l. The elastic force of the cantilever tip will act as a counterbalance to the force caused by the torque. In this way:

$$\vec{\tau} = \vec{F} \times \vec{l}, \tag{5}$$

or:

$$\tau = k\Delta x \cdot l, \tag{6}$$

where k is a spring constant of the cantilever and Δx is a deflection at the edge of cantilever. Comparing Equations 4 and 6, we obtain an expression that relates the deviation of the tip of the cantilever with the magnetic field and angle:

$$k\Delta x \cdot l = \frac{1}{2} \chi_{\parallel} m_m B^2 \sin(2\theta), \longrightarrow \tag{7}$$

$$\chi_{\parallel} = \frac{2kl}{m_m} \frac{\Delta x}{B^2 \sin(2\theta)} \tag{8}$$

For the cantilevers that have a piezoresistor as a pressure sensor, the calibration parameter is found as a gauge factor (GF), which shows the relative variation of the piezoresistance with respect to the relative deflection of the cantilever [23–26]:

$$\frac{\Delta R}{R_0} = GF \frac{\Delta x}{l}, \tag{9}$$

where R_0 is the resistance of the piezoresistor in the undeflected state.

With Equations (8) and (9), we obtain a general formula for the calculation of the susceptibility of an anisotropic sample as:

$$\chi_{\parallel} = \frac{\Delta R}{R_0 GF} \frac{2kl^2}{m_m B^2 \sin(2\theta)} \tag{10}$$

To determine the susceptibility of the graphite samples, we used the cantilevers with an integrated Wheatstone bridge, which has four piezoresistors, and two of them are placed at the bottom of the cantilever tip. To measure the change of resistance of the piezoresistor ΔR, we used the AC resistor bridge. In this configuration, the measured resistance is related to the change in the resistance of the piezoresistor as $\Delta R = 2R_{meas}$. Based on the above given expressions, the final formula for the susceptibility of an anisotropic sample in the used experimental setup:

$$\chi_{\parallel} = \frac{2R_{meas}}{R_0 GF} \frac{2kl^2}{m_m B^2 \sin(2\theta)} \tag{11}$$

The measured R_{meas} of three graphite samples are presented in Figure S3. The typical values of the spring constants of the used cantilevers are k = 8–23 N/m (see the Table 1). To calculate the spring constant k, we used the equation from [27]:

$$k = \frac{E t_c^3 w}{4l^3}, \tag{12}$$

where w is the width and l is the length of the cantilever tip, t_c is the cantilever thickness, and $E = 1.7 \cdot 10^{11}$ Pa the Young's modulus.

The values of the gauge factor *GF* (Table 1) for each cantilever were mechanically obtained using an optical microscope and a micromanipulator from SURUGA SEIKI CO., LTD, following the method reported in [23]. The needle of the micromanipulator was lowered in steps of 0.1–1 μm and pressed at the edge of the cantilever. The change in the resistance of the piezoresistor on the cantilever was recorded by the AC resistance bridge. To test the accuracy of mechanical calibrations, we carried out an additional calibration with the HOPG sample of thickness 30.6 μm measured in an SQUID magnetometer and a torque magnetometer. Both calibrations turned out to be identical, within the slight non-linearity of the torque magnetometer; see Figure S4.

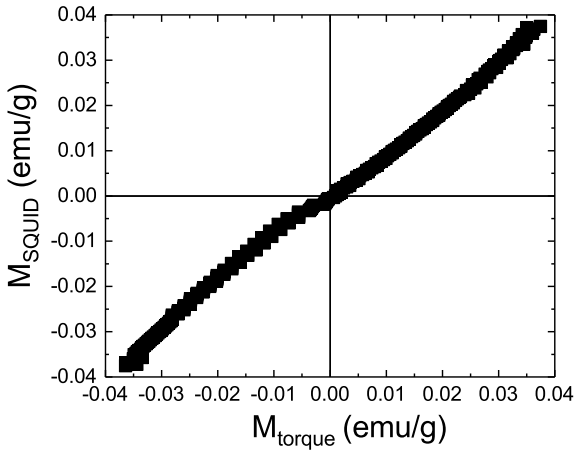

Figure S4. Magnetization of the HOPG sample of thickness 30.6 μm, obtained with a SQUID magnetometer and a torque magnetometer.

Additional experimental data and characterization of the used cantilevers can be seen in [28].

5. Influence of Substrate on the SQUID Measurements

In order to avoid the influence of spurious contributions to the magnetic measurements of the graphite samples in the SQUID magnetometer, we used a thin silicon substrate ($4 \times 4 \times 0.18$ mm^3). The value of the magnetic moment of the silicone substrate was $\sim 10^{-6}$ emu under an applied magnetic field of 10 kOe. The value of the smallest magnetic moment of a graphite sample with a thickness 7.7 μm was of the order of 10^{-5} emu under the same applied magnetic field.

1. Zoraghi, M.; Barzola-Quiquia, J.; Stiller, M.; Setzer, A.; Esquinazi, P.; Kloess, G.H.; Muenster, T.; Lühmann, T.; Estrela-Lopis, I. Influence of rhombohedral stacking order in the electrical resistance of bulk and mesoscopic graphite. *Phys. Rev. B* **2017**, *95*, 045308. doi:10.1103/PhysRevB.95.045308.
2. Krishnan, K.S. Magnetic Anisotropy of Graphite. *Nature* **1934**, *133*, 174–175. doi:10.1038/133174c0.
3. Ganguli, N. Magnetic studies on graphite and graphitic oxides. *The London, Edinburgh, and Dublin Philosophical Magazine and Journal of Science* **1936**, *21*, 355–369. doi:10.1080/14786443608561589.
4. Fischbach, D.B. Diamagnetic Susceptibility of Pyrolytic Graphite. *Phys. Rev.* **1961**, *123*, 1613–1614. doi:10.1103/PhysRev.123.1613.
5. Simon, M.D.; Geim, A.K. Diamagnetic levitation: Flying frogs and floating magnets (invited). *Journal of Applied Physics* **2000**, *87*, 6200–6204. doi:10.1063/1.372654.
6. Sepioni, M.; Nair, R.R.; Rablen, S.; Narayanan, J.; Tuna, F.; Winpenny, R.; Geim, A.K.; Grigorieva, I.V. Limits on Intrinsic Magnetism in Graphene. *Phys. Rev. Lett.* **2010**, *105*, 207205. doi:10.1103/PhysRevLett.105.207205.
7. Tongay, S.; Hwang, J.; Tanner, D.B.; Pal, H.K.; Maslov, D.; Hebard, A.F. Supermetallic conductivity in bromine-intercalated graphite. *Phys. Rev. B* **2010**, *81*, 115428. doi:10.1103/PhysRevB.81.115428.

8. Miao, X.; Tongay, S.; Hebard, A.F. Extinction of ferromagnetism in highly ordered pyrolytic graphite by annealing. *Carbon* **2012**, *50*, 1614 – 1618. doi:https://doi.org/10.1016/j.carbon.2011.11.040.
9. Iye, Y.; Tedrow, P.M.; Timp, G.; Shayegan, M.; Dresselhaus, M.S.; Dresselhaus, G.; Furukawa, A.; Tanuma, S. High-magnetic-field electronic phase transition in graphite observed by magnetoresistance anomaly. *Phys. Rev. B* **1982**, *25*, 5478–5485. doi:10.1103/PhysRevB.25.5478.
10. Barzola-Quiquia, J.; Yao, J.L.; Rödiger, P.; Schindler, K.; Esquinazi, P. Sample Size Effects on the Transport Characteristics of Mesoscopic Graphite Samples. *phys. stat. sol. (a)* **2008**, *205*, 2924–2933. doi:10.1002/pssa.200824288.
11. Esquinazi, P.; García, N.; Barzola-Quiquia, J.; Rödiger, P.; Schindler, K.; Yao, J.L.; Ziese, M. Indications for intrinsic superconductivity in highly oriented pyrolytic graphite. *Phys. Rev. B* **2008**, *78*, 134516. doi:10.1103/PhysRevB.78.134516.
12. Ocaña, R.; Esquinazi, P.; Kempa, H.; Torres, J.H.S.; Kopelevich, Y. Magnetothermal conductivity of highly oriented pyrolytic graphite in the quantum limit. *Phys. Rev. B* **2003**, *68*, 165408. doi:10.1103/PhysRevB.68.165408.
13. Kim, J.; Kim, D.; Lee, K.W.; Choi, E.; Noh, S.; Kim, H.; Lee, C.E. Proton-irradiation effects on the charge transport in highly oriented pyrolytic graphite. *Solid State Communications* **2014**, *186*, 5 – 7. doi:https://doi.org/10.1016/j.ssc.2014.01.023.
14. García, N.; Esquinazi, P.; Barzola-Quiquia, J.; Dusari, S. Evidence for semiconducting behavior with a narrow band gap of Bernal graphite. *New Journal of Physics* **2012**, *14*, 053015. doi:10.1088/1367-2630/14/5/053015.
15. Esquinazi, P.D.; Lysogorskiy, Y., Basic Physics of functionalized graphite; Springer Series in Materials Science 244, P. Esquinazi (ed.), Springer International Publishing AG Switzerland, 2016; chapter 7, pp. 145–179. doi:10.1007/978-3-319-39355-1.
16. Spemann, D.; Esquinazi, P.; Setzer, A.; Böhlmann, W. Trace element content and magnetic properties of commercial HOPG samples studied by ion beam microscopy and SQUID magnetometry. *AIP Advances* **2014**, *4*, 107142. doi:https://doi.org/10.1063/1.4900613.
17. Precker, C.E.; Esquinazi, P.D.; Champi, A.; Barzola-Quiquia, J.; Zoraghi, M.; Muiños-Landin, S.; Setzer, A.; Böhlmann, W.; Spemann, D.; Meijer, J.; Muenster, T.; Baehre, O.; Kloess, G.; Beth, H. Identification of a possible superconducting transition above room temperature in natural graphite crystals. *New J. Phys.* **2016**, *18*, 113041. doi:https://doi.org/10.1088/1367-2630/18/11/113041.
18. Esquinazi, P.; Barzola-Quiquia, J.; Dusari, S.; García, N. Length dependence of the resistance in graphite: Influence of ballistic transport. *J. Appl. Phys.* **2012**, *111*, 033709. doi:https://doi.org/10.1063/1.3682094.
19. García, N.; Esquinazi, P.; Barzola-Quiquia, J.; Ming, B.; Spoddig, D. Transition from Ohmic to ballistic transport in oriented graphite: Measurements and numerical simulations. *Phys. Rev. B* **2008**, *78*, 035413. doi:10.1103/PhysRevB.78.035413.
20. Dusari, S.; Barzola-Quiquia, J.; Esquinazi, P.; García, N. Ballistic transport at room temperature in micrometer-size graphite flakes. *Phys. Rev. B* **2011**, *83*, 125402. doi:https://doi.org/10.1103/PhysRevB.83.125402.
21. Spemann, D.; Esquinazi, P.D., Evidence for Magnetic Order in Graphite from Magnetization and Transport Measurements. In *Basic Physics of Functionalized Graphite*; Esquinazi, P.D., Ed.; Springer International Publishing: Cham, 2016; pp. 45–76. doi:10.1007/978-3-319-39355-1_3.
22. Torizuka, K.; Tajima, H.; Yoshida, G.; Inoue, M. Calibration Technique Using Nonlinear Region in Cantilever Magnetometry Experiments and Presence of Universal Curve. *Japanese Journal of Applied Physics* **2013**, *52*, 066601. doi:10.7567/JJAP.52.066601.
23. Seto, J.Y.W. Piezoresistive properties of polycrystalline silicon. *Journal of Applied Physics* **1976**, *47*, 4780–4783. doi:10.1063/1.322515.
24. Kanda, Y. Piezoresistance effect of silicon. *Sensors and Actuators A: Physical* **1991**, *28*, 83 – 91. doi:https://doi.org/10.1016/0924-4247(91)85017-I.
25. Yu, X.; Thaysen, J.; Hansen, O.; Boisen, A. Optimization of sensitivity and noise in piezoresistive cantilevers. *Journal of Applied Physics* **2002**, *92*, 6296–6301. doi:10.1063/1.1493660.
26. Barlian, A.A.; Park, W.T.; Mallon, J.R.; Rastegar, A.J.; Pruitt, B.L. Review: Semiconductor Piezoresistance for Microsystems. *Proceedings of the IEEE* **2009**, *97*, 513–552. doi:10.1109/JPROC.2009.2013612.

27. Cleveland, J.P.; Manne, S.; Bocek, D.; Hansma, P.K. A nondestructive method for determining the spring constant of cantilevers for scanning force microscopy. *Review of Scientific Instruments* **1993**, *64*, 403–405. doi:10.1063/1.1144209.
28. Stavrov, V.; Stavreva, G.; Tomerov, E.; Todorov, V.; Buchvarov, I. In-line thickness control of self-sensing cantilevers for advanced AFM applications. 2017 40th International Spring Seminar on Electronics Technology (ISSE), 2017, pp. 1–4. doi:10.1109/ISSE.2017.8000890.